

Article

Nanocomposite of MgFe_2O_4 and Mn_3O_4 as Polyphenol Oxidase Mimic for Sensing of Polyphenols

Harmilan Kaur¹, Manpreet Kaur^{1,*} , Renuka Aggarwal², Sucheta Sharma³ and Davinder Singh⁴¹ Department of Chemistry, Punjab Agricultural University, Ludhiana 141004, India; harmilan2020-cm@pau.edu² Department of Food and Nutrition, Punjab Agricultural University, Ludhiana 141004, India; renukaaggarwal@pau.edu³ Department of Biochemistry, Punjab Agricultural University, Ludhiana 141004, India; suchetasharma_pau@pau.edu⁴ Department of Extension Education, Punjab Agricultural University, Ludhiana 141004, India; davinder-ee@pau.edu

* Correspondence: manpreetchem@pau.edu

Abstract: Polyphenol oxidase (PPO) mimics have advantage of detection and remediation of polyphenols. This work demonstrates rapid and sensitive colorimetric detection of phenolic compounds using nanocomposite of magnesium ferrite (MgFe_2O_4) and manganese oxide (Mn_3O_4) nanoparticles as PPO mimic. The catalytic properties of MgFe_2O_4 and Mn_3O_4 displayed synergistic effect in the nanocomposite. The synthesized nanocomposite and nanoparticles were fully characterized using various analytical techniques. The ratio of MgFe_2O_4 and Mn_3O_4 in the nanocomposite was optimized. Catechol and resorcinol were taken as model polyphenols. The best PPO-activity was shown by $\text{MgFe}_2\text{O}_4@\text{Mn}_3\text{O}_4$ nanocomposite with of w/w ratio 1:2. The results correlated with its higher surface area. Reaction parameters viz. pH, temperature, contact time, substrate concentration, and nanoparticles dose were studied. The synthesized $\text{MgFe}_2\text{O}_4@\text{Mn}_3\text{O}_4$ nanocomposite was used for the detection of catechol in the linear range of 0.1–0.8 mM with the detection limit of 0.20 mM, and resorcinol in the range of 0.01–0.08 mM with the detection limit of 0.03 mM. The estimated total phenolic content of green and black tea correlated well with the conventional method. These results authenticate promising future potential of $\text{MgFe}_2\text{O}_4@\text{Mn}_3\text{O}_4$ nanocomposite as PPO-mimic

Keywords: polyphenol oxidase mimic; catechol sensing; resorcinol sensing; $\text{MgFe}_2\text{O}_4@\text{Mn}_3\text{O}_4$ NCs

Citation: Kaur, H.; Kaur, M.; Aggarwal, R.; Sharma, S.; Singh, D. Nanocomposite of MgFe_2O_4 and Mn_3O_4 as Polyphenol Oxidase Mimic for Sensing of Polyphenols. *Biosensors* **2022**, *12*, 428. <https://doi.org/10.3390/bios12060428>

Received: 19 May 2022

Accepted: 15 June 2022

Published: 17 June 2022

Publisher's Note: MDPI stays neutral with regard to jurisdictional claims in published maps and institutional affiliations.



Copyright: © 2022 by the authors. Licensee MDPI, Basel, Switzerland. This article is an open access article distributed under the terms and conditions of the Creative Commons Attribution (CC BY) license (<https://creativecommons.org/licenses/by/4.0/>).

1. Introduction

The term “enzyme mimic” refers to a synthetic enzyme that performs similar functions as its natural analogue. Natural enzymes have higher catalytic efficiency, are substrate specific and are widely employed in the food processing sectors. However, they are prone to temperature and pH changes, which causes denaturation [1]. Enzyme mimics are being studied to circumvent these limitations of natural enzymes. Nanoparticles (NPs) are tiny particles having diameter ranging from 1 nm to 100 nm [2]. They differ from the bulk material in terms of catalytic properties and have a wide range of biological and catalytic applications [3]. Nanozymes, or NPs with enzyme-like properties, have been studied for their potential applications in biosensors, pharmaceutical and food sectors [4]. Nanozymes come in a variety of shapes and sizes, including rods, fibers, wires, tubes, and nanopopcorns, all of which have inherent capabilities to operate as enzyme mimics [5–7]. Magnesium ferrite (MgFe_2O_4) is a stable material with catalytic and magnetic properties. The flower-like $\text{MoS}_2@\text{MgFe}_2\text{O}_4$ composites have been reported to simulate peroxidase activity [8,9]. Polyphenol oxidase mimics have immense potential for detecting phenolic substances such as catechol and resorcinol [10–13]. Due to their stability, toxicity, and carcinogenicity, phenols have been identified as hazardous water pollutant [14]. As a result, monitoring phenols in the environment is an important aspect of research. Although analysis methods,

viz chemiluminescence and fluorometry have been developed for the detection of phenols with high sensitivity, they all have the inherent shortcoming of qualitative identification for phenols [15–17]. Electrochemical methods for the determination of phenolic compounds (e.g., catechin) too are preferred over other methods because of their fast response time, low detection limit and relatively low cost [18–20]. Chromatography and mass spectrometry have been used to identify and detect phenols with high accuracy and sensitivity, but they require expensive instruments and time-consuming operations, making them unsuitable for rapid analysis. Colorimetric approach, in comparison to other outlined methods, do not necessitate considerable instrumentation or preprocessing, and is also less expensive. It also offers the benefit of being able to analyze the data using visual detection [21]. Colorimetry has recently been devised for the assay of phenols based on nanozyme activity and received a lot of interest in the biological and environmental science due to its advantages of being simple and intuitive [22–24]. Different NPs with polyphenol oxidase mimicking activity are studied in the sensing applications. Ferrite NPs have piqued the interest of researchers due to their usage in bio-applications. They are ceramic materials made by physical and chemical blending of iron (III) oxide with modest amounts of other elements. The size, chemical composition, and particle interaction with the surrounding matrix all influence the properties of ferrite NPs [25–27]. To identify polyphenols, we have proposed a facile colorimetric method based on the polyphenol oxidase-mimicking activity of $\text{MgFe}_2\text{O}_4@\text{Mn}_3\text{O}_4$ nanocomposite. Catechol and resorcinol were taken as model polyphenols as they are commonly used and are easily available. Furthermore, in the quantitative colorimetric detection of catechol and resorcinol, the newly devised approach exhibits good sensitivity. This method, which is based on PPO-like activity of nanocomposite $\text{MgFe}_2\text{O}_4@\text{Mn}_3\text{O}_4$, shows tremendous promise for monitoring phenols in the environment. The research was extended to application of synthesized nanocomposite for colorimetric detection of polyphenols in the tea samples in order to assess the antioxidant effectiveness of foods rich in phenolics and define their perspective potential [28]. MgFe_2O_4 NPs and Mn_3O_4 NPs were synthesized using the sol-gel method, whereas the nanocomposite was fabricated using the ultrasonication method. Sol-gel synthesis provides numerous benefits over traditional approaches for producing high-quality NPs with uniformity and purity. It operates at low temperatures and has ability to produce fine powders [26]. Ultrasonication approach helps in fine blending of the NPs in the nanocomposite. The synthesized NPs and nanocomposite were fully characterized and effect of various parameters on enzyme mimic activity of $\text{MgFe}_2\text{O}_4@\text{Mn}_3\text{O}_4$ nanocomposite. The present work highlights the PPO-mimic potential of synthesized nanocomposite for detecting polyphenols.

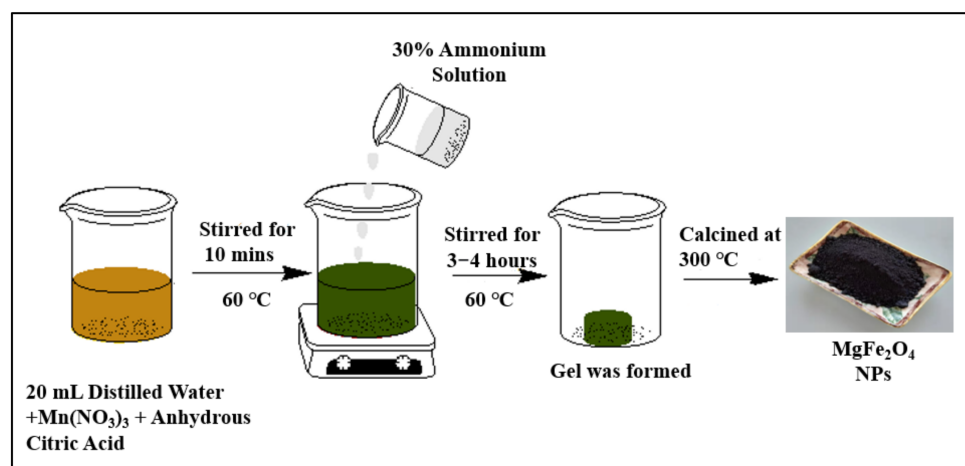
2. Experimental

2.1. Materials and Reagents

All of the chemicals utilized were of analytical quality, viz. magnesium nitrate hexahydrate ($\text{Mg}(\text{NO}_3)_2 \cdot 6\text{H}_2\text{O}$), ferric nitrate nonahydrate ($\text{Fe}(\text{NO}_3)_3 \cdot 9\text{H}_2\text{O}$), citric acid monohydrate ($\text{C}_6\text{H}_8\text{O}_7\text{H}_2\text{O}$), ammonium hydroxide (NH_4OH), manganese nitrate tetrahydrate ($\text{Mn}(\text{NO}_3)_2 \cdot 4\text{H}_2\text{O}$), catechol ($\text{C}_6\text{H}_6\text{O}_2$), and resorcinol ($\text{C}_6\text{H}_6\text{O}_2$). Deionized water was used for preparing the solutions.

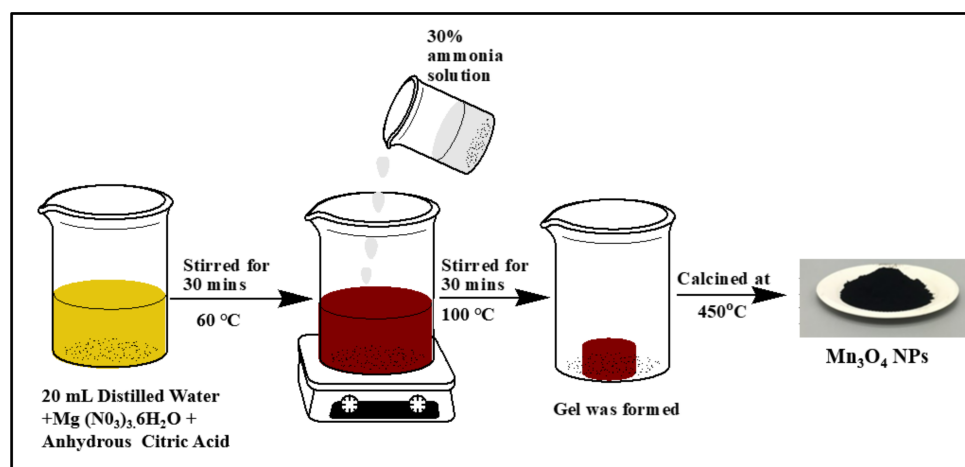
2.2. Synthesis of MgFe_2O_4 NPs, Mn_3O_4 NPs, and $\text{MgFe}_2\text{O}_4@\text{Mn}_3\text{O}_4$ NC and Its Characterization

MgFe_2O_4 NPs were synthesized using sol-gel method where citric acid is used as a chelating agent (Scheme 1) [29]. In 2:1 molar ratio, ferric nitrate (2.0 mol) and magnesium nitrate (1.0 mol) were dissolved in deionized water, followed by the addition of 4.5 mol citric acid to the reaction mixture. By adding ammonium hydroxide, the pH of the solution was neutralized, and the solution was turned into gel after continuous stirring at 60 °C for 4 h. The gel was dried at 160 °C and calcined for 3 h at 300 °C. These NPs were labelled as H-1 NPs.



Scheme 1. Synthesis of magnesium ferrite nanoparticles using sol-gel method.

Sol-gel method was used to synthesize Mn₃O₄ NPs. In 20 mL distilled water, Mn(NO₃)₂ (0.09 mol) and citric acid (0.05 mol) were dissolved (Scheme 2). The aforementioned mixture was magnetically agitated at 60 °C, and 20 mL of ammonium hydroxide (30% NH₄OH) was added to neutralize it. The sol was converted into gel after 12 h of stirring. The gel was dried at 100 °C for overnight with increased volume. The gel was calcined at 450 °C for 3 h to acquire Mn₃O₄ NPs. These NPs were designated as H-2 NPs



Scheme 2. Synthesis of manganese oxide nanoparticles using sol-gel method.

The nanocomposites (NC) of MgFe₂O₄ and Mn₃O₄ with *w:w* ratio of MgFe₂O₄:Mn₃O₄, i.e., 2:1 and 1:2 was synthesized by facile ultrasonication method. The synthesized MgFe₂O₄ and Mn₃O₄ NPs were sonicated separately in deionized water for 20 min. These two solutions were mixed and sonicated for 1 h which were designated as H-3 and H-4 NCs, respectively. H-4 NC displayed the best enzyme mimic activity as compared to H-3 NC and pristine H-1 and H-2 NPs, so rest of the experiments were performed using H-4 NC. Table S1, lists the characterization tools used to evaluate surface morphology, particle size, phase purity, functional groups, and magnetic properties.

2.3. PPO-Mimic Activity and Kinetic Analysis

Zauberman method was used to assess the PPO-like activity of synthesized NPs. PPO catalyzes the oxidation of polyphenols to their respective o-quinones [27,30]. Nanocomposite was used instead of PPO utilizing catechol and resorcinol as substrates. 1 mg of synthesized NPs and 3.5 mL of 3 mM catechol/resorcinol solution at pH 3.0 were added to the reaction mixture. Activity of nanocomposite was assessed under different conditions of

pH (1.0–7.0), temperature (10–50 °C), substrate concentration (1–5 mM), and enzyme mimic dosage (1–7 mg). The contact time was investigated up to 40 min. Each set of experimental data was optimized using the Box-Behnken methodology using design expert software (version 11).

The reaction kinetics was studied at 25 °C. The quantity of catechol and resorcinol was increased from 1 mM to 6 mM, and 5 mg of nanocomposite was added at an optimal pH of 3.0 with the addition of 0.5 mL H₂O₂ into each solution. The absorbance at 390 nm was measured at 1-min intervals for 5 min. From the Lineweaver-Burk plot, the Michaelis-Menton constant was determined as follows:

$$\frac{1}{V} = \frac{K_m}{V_{max}[S]} + \frac{1}{V_{max}} \quad (i)$$

where

“V” stands for reaction rate,

V_{max} for maximum velocity of reaction,

S is the substrate concentration, and

K_m stands for Apparent Michaelis constant, which indicates the affinity of enzyme or enzyme mimic for its substrate. Lower value of K_m corresponds to higher efficiency of catalyst.

2.4. Box-Behnken Approach for Atatistical Analysis

The current study used the Box-Behnken experimental design approach to investigate and standardise the following factors on enzyme activity: pH (A); Temperature (B); Catalyst dosage (C); Contact time (D). The Box-Behnken experimental design method establishes a mathematical link between components and experimental data, which can subsequently be fitted to a second-order polynomial model as the equation. As a result, Equation (1) is proposed for creating a mathematical correlation between enzyme activity and the four independent parameters chosen [31]. This equation is particularly useful in analyzing the impact of four selected experimental factors on the enzyme activity of MgFe₂O₄@Mn₃O₄ (1:2) nanocomposite and determining the optimum values.

$$\text{Absorbance} = \beta_0 + \beta_1A + \beta_2B + \beta_3C + \beta_4D + \beta_5AB + \beta_6AC + \beta_7AD + \beta_8BC + \beta_9BD + \beta_{10}CD + \beta_{11}A^2 + \beta_{12}B^2 + \beta_{13}C^2 + \beta_{14}D^2 \quad (1)$$

where β_0 , β_{ii} , β_{ij} are the model's constant, linear, quadratic, and interaction coefficients. The Design-Expert Software was used to determine these constants (Version XI). Notably, the suggested model's quality and goodness Equation (1), as well as the coefficient of determination (R^2), were calculated. Aside from that, the residuals' normal distribution was employed, as well as a plot of actual vs expected values. Analysis of variance (ANOVA) was used for statistical response analysis, with a p -value of 0.05 assumed to demonstrate the statistical significance of the proposed model's parameters. Based on the experimental design, Table S2 (Given in the supplementary data) indicates the range and levels of the components.

2.5. Detection of Catechol and Resorcinol Based on MgFe₂O₄@Mn₃O₄ (1:2) Polyphenol Oxidase

Catechol detection was accomplished as follows:

100 μ L of MgFe₂O₄@Mn₃O₄ (0.25 mg mL⁻¹) solution was mixed with various concentrations of catechol (0.1–0.8 mM) solution at pH 3.0. The absorbance at 390 nm was measured after 10 min of incubation at 25 °C.

Resorcinol detection was accomplished as follows:

100 μ L of MgFe₂O₄@Mn₃O₄ (0.25 mg mL⁻¹) solution was mixed with various concentrations of resorcinol (0.01–0.08 mM) solution at pH 3.0. The absorbance at 390 nm was measured after incubating the solution at 25 °C for 10 min.

2.6. Detection of Polyphenols in Tea Samples Based on $\text{MgFe}_2\text{O}_4@\text{Mn}_3\text{O}_4$ (1:2) Polyphenol Oxidase Mimic

To estimate total phenol content, the Folin-Ciocalteu method was employed, which entailed mixing 20 μL of adequately diluted green and black tea extract (or phenolic standard) with 20 μL of Folin-Ciocalteu reagent for 3 min. Then, to make a total capacity of 1000 μL , 400 μL of sodium carbonate (7.5 percent Na_2CO_3) and deionized water were added. The solution was stirred for 60 min at room temperature in the dark, and the total polyphenolic content was determined using a spectrophotometer. The total phenolic content measured by the Folin-Ciocalteu assay was statistically correlated with the results from the study of two different tea types using for green and black tea by using optimized conditions of $\text{MgFe}_2\text{O}_4 @\text{Mn}_3\text{O}_4$ NC. Gallic acid (concentration range 20–100 $\mu\text{g}/\text{mL}$) was used as a standard for preparing calibration curve (Figure S10). Take different concentration of gallic acid followed by the addition of 5 mg of synthesized NC and 0.5 mL of H_2O_2 at $\text{pH} = 3$. Total volume was made 10 mL using distilled water. The value of absorbance corresponding to each test tube was noted to plot the calibration curve. The sample was prepared by adding 0.2 mL green and black tea extracts followed by the addition of 5 mg of NC and 0.5 mL H_2O_2 at $\text{pH} = 3$. The total volume of test sample was made 10 mL with the help of distilled water and total phenolic content was determined.

2.7. Recyclability Test

For the PPO-mimic reusability, 20 mL, 2 mM substrate at optimal pH of 3.0 was taken. 5 mg synthesized nanocomposite was added in the solution and the absorbance was measured at 390 nm after 10 min of incubation at 25 °C. The nanocomposite was then rinsed many times with deionized water. For the second cycle, the nanocomposite was centrifuged and dried in oven at 100 °C. This cycle was repeated four times.

3. Results and Discussions

3.1. Characterization of Synthesized NPs

3.1.1. Structural Analysis

XRD was used to identify phase and purity of synthesized NPs and nanocomposites. X-ray diffractograms displayed well defined peaks (Figure 1) and XRD parameters are listed in Table 1. The XRD pattern of H-1 NPs exhibited peaks at $2\theta = 30.12^\circ, 35.48^\circ, 43.11^\circ, 53.54^\circ, 57.05^\circ$ and 62.63° which were associated with (220), (311), (400), (422), (511) and (440) planes [32,33]. These planes associated with the peaks proved to be strong evidence of the successful synthesis of MgFe_2O_4 . Moreover, the absence of the extra peaks in the pattern made it evident that the synthesis of MgFe_2O_4 NPs were in pure phase. The diffraction pattern of H-2 NPs showed sharp peaks at $2\theta = 18.07^\circ, 28.96^\circ, 31.10^\circ, 32.40^\circ, 36.10^\circ, 38.22^\circ, 44.44^\circ, 50.95^\circ, 53.88^\circ, 56.05^\circ, 58.64^\circ, 60.03^\circ$ and 64.73° corresponding to crystallographic planes (101), (112), (200), (103), (211), (004), (220), (105), (312), (303), (321), (324) and (400), respectively. The sharp diffraction peaks revealed that the NPs were well crystalline in nature. The combined peaks of H-1 and H-2 NPs were seen in the XRD patterns of H-3 and H-4, thus confirming its presence in the nanocomposite.

Fourier Transformation Infrared (FT-IR) was employed for studying functionalities in the synthesized NPs as illustrated in Figure S1. In case of H-1 NPs the band at 3424 cm^{-1} was assigned to O-H stretching and the band at 1633 cm^{-1} was accredited to O-H bending vibrations. Strong bands at 578 cm^{-1} and 480 cm^{-1} were observed confirming the formation of spinel structure. In addition, the band at 578 cm^{-1} were ascribed to the metal-oxygen bond vibrations in the tetrahedral lattice sites. Meanwhile, bands observed at lower frequency were assigned to metal-oxygen bond vibrations in the octahedral sites. The greater mass of Mn^{3+} ions in Mn_3O_4 resulted in higher band frequency as compared to MgFe_2O_4 . The FT-IR spectrum of H-2 NPs showed a broad band at 3400 cm^{-1} and a narrow band at 1631 cm^{-1} due to stretching and bending vibrations of adsorbed water molecules. The small noticeable bands at 1384 cm^{-1} can be due to the presence of residues of nitrate whereas band at 1121 cm^{-1} can be ascribed to C-OH stretching [34]. The band at 606 cm^{-1}

was created by Mn-O stretching modes at tetrahedral sites, while the band at 487 cm^{-1} was caused by Mn-O distortion vibration in an octahedral environment [35–37]. The vibration of manganese species (Mn^{3+}) in the octahedral sites caused the third band to be positioned at a weaker wave number 422 cm^{-1} . The peaks of H-1 and H-2 NPs were observed in the spectra of H-3 and H-4 nanocomposites, confirming the presence of nanocomposite.

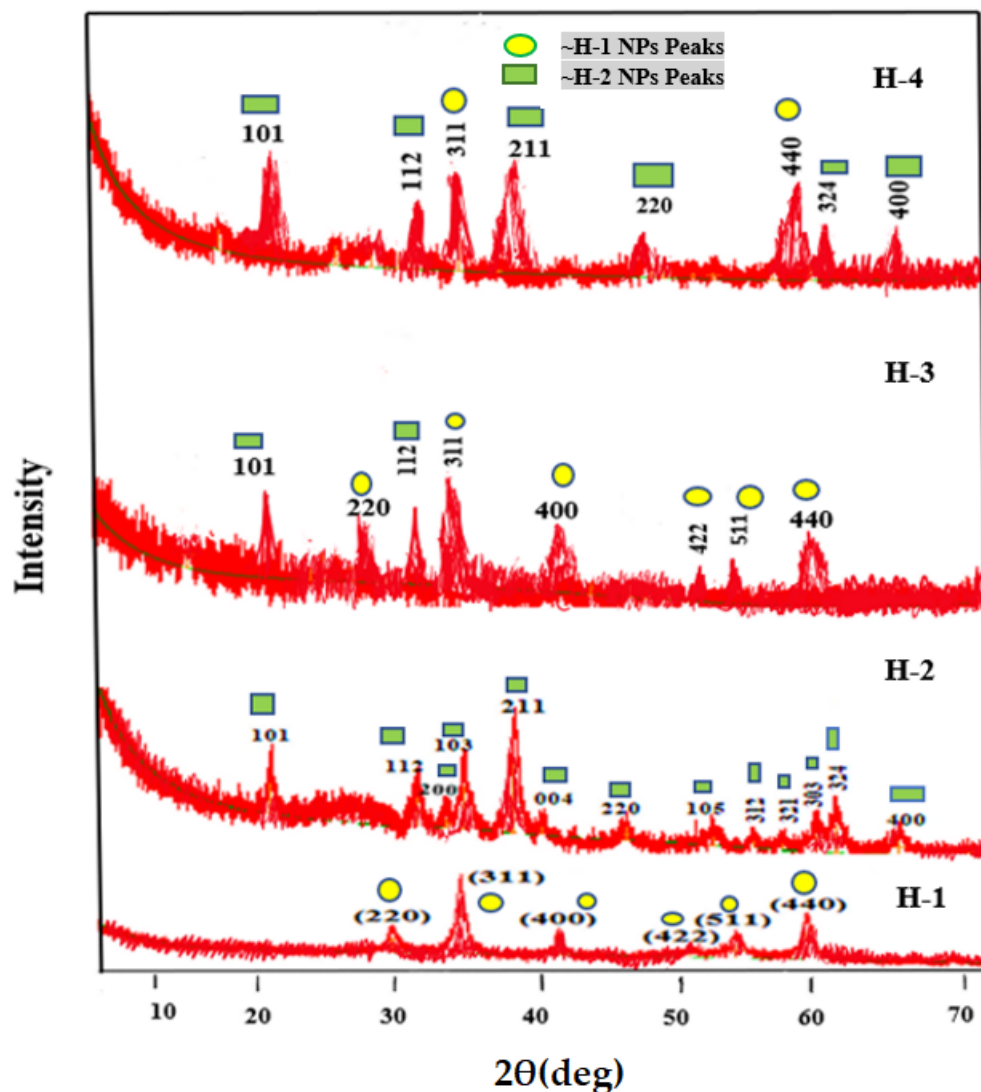


Figure 1. X-ray diffraction patterns of H-1, H-2, H-3 and H-4 NPs.

Table 1. XRD Parameters of Nanoparticles.

Material Abbreviation	(NPs)	Lattice Constant (Å)	Average Particle Diameter (nm)	XRD Density g/cc
H-1	MgFe_2O_4	8.40	11.0	4.5
H-2	Mn_3O_4	5.95	15.0	14.4

3.1.2. Morphological and Magnetic Studies

SEM image of H-1 NPs (Figure S2a) showed voids and pores as a result of gases released during gel combustion. Due to their magnetic nature and binding of primary particles via weak surface interactions such as van der Waals forces, ferrite NPs displayed a substantial degree of agglomeration. The presence of oxygen, iron and magnesium

elements with compositions of 56.44%, 29.63%, and 13.94%, respectively, was observed in the EDS spectrum of H-1 NPs. Figure S2b display SEM image of H-2 NPs which looks similar to irregular three-dimensional distorted nano-spheres. In addition, EDS recorded for Mn_3O_4 confirmed the presence of manganese and oxygen with composition of 72.79% and 24.76%, respectively. In case of H-3 and H-4 nanocomposites, (Figures 2 and S2c) with the immobilization of NPs, the surface had a rough appearance, indicating low aggregation and consequently excellent dispersion. In addition, EDS of H-3 and H-4 NCs confirmed the presence of magnesium, manganese, iron and oxygen [38].

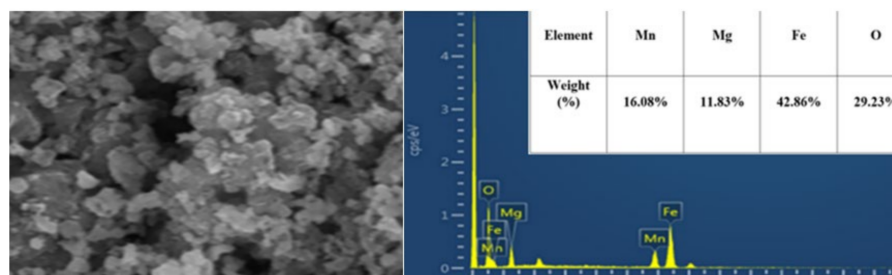


Figure 2. SEM-EDS of H-4 nanocomposite.

TEM imaging (Figure S3a,b) was used to study the average particle size and aggregation behaviour of the pristine MgFe_2O_4 and Mn_3O_4 NPs. Distribution of size and morphology of the synthesized NPs was specified employing TEM analysis. MgFe_2O_4 NPs exhibited agglomeration in TEM image which is typical characteristic of magnetic NPs. The highest proportion of particles had a size in the range of 40–50 nm. TEM of Mn_3O_4 NPs shows spherical shaped particles having particle size in the range between 10–20 nm which was similar to as found through XRD studies [23].

Hysteresis plots displaying the altering of magnetization (M_s , emu g^{-1}) as an effect of applied magnetic field (H , Oe) is illustrated in Figure 3. The magnetic character of the H-1 NPs depends crucially on the size, shape and purity of the NPs. It is very interesting that MgFe_2O_4 shows magnetism even though Mg^{2+} ions are non-magnetic. This can be ascribed to the incomplete inverse spinel structure of MgFe_2O_4 . The H-2 NPs showed linear behaviour in M – H curves, indicating their paramagnetic character at 300 K as shown in Figure 3. Hysteresis plot in single-domain ferrimagnetic particles vanishes when particle size becomes so small that the maximum anisotropy energy becomes close to the thermal energy, and the process of flipping of the single domain spin becomes inhibited. These types of particles do not possess any coercivity and their magnetization never becomes saturated even at very high applied field [26,36,37]. The presence of hysteresis loop indicates that particles are multidomain in the present studies. At room temperature, the ferrite NPs displayed s-shaped thin hysteresis loop, indicating their ferrimagnetic nature. The M_s values for H-1, H-2, H-3 and H-4 were 23.34 emu g^{-1} , 0.86 emu g^{-1} , 19.53 emu g^{-1} , 18.48 emu g^{-1} and 18.34 emu g^{-1} . The saturation magnetization values of H-3 NC decreased in comparison to pure H-1 NPs. This fall in M_s value was assigned to the presence of non-magnetic Mn_3O_4 in H-3 and H-4 NC which influences the magnetization as a result of quenching magnetic momentum. The surface imperfections of the ferrite NPs also contribute to the drop in M_s values. The values of coercivity drop as the presence of manganese ion in H-3 and H-4 increases. The other magnetic parameters, i.e., the remanence magnetization (M_r) also falls with the addition of nonmagnetic Mn^{3+} ions (Table 2). The narrow loops hinted the low coercivity values which implies that the synthesized ferrites could be demagnetized easily.

The BET surface area of H-1, H-2, H-3 and H-4 NPs was recorded as $32.81 \text{ m}^2\text{g}^{-1}$, $38.98 \text{ m}^2\text{g}^{-1}$, $53.03 \text{ m}^2\text{g}^{-1}$, and $70.17 \text{ m}^2\text{g}^{-1}$, respectively. The total pore volume of H-1, H-2, H-3 and H-4 was 0.030 cc g^{-1} , 0.122 cc g^{-1} , 0.17 cc g^{-1} , and 0.18 cc g^{-1} , respectively. According to the IUPAC classification, representative of mesoporous structures, all samples exhibited typical type-IV isotherms with hysteresis loop of H4 type and therefore depicting

the slit shaped pores. The BJH pore size distribution displayed one narrow peak centred at 3.59 nm and 6.59 nm for H-1 and H-2 NPs, respectively. H-3 and H-4 exhibited the unimodal pore size distribution as well displaying peaks centred at 11.32 nm and 16.47 nm, respectively [39]. The H-3 and H-4 NC exhibited higher surface area as well as pore volumes explaining the enzyme mimic activity. With increasing Mn_3O_4 content the surface area increased from $53.03 \text{ m}^2\text{g}^{-1}$ for H-3 NC to $70.17 \text{ m}^2\text{g}^{-1}$ for H-4 NC (Figure 4 and Table 3).

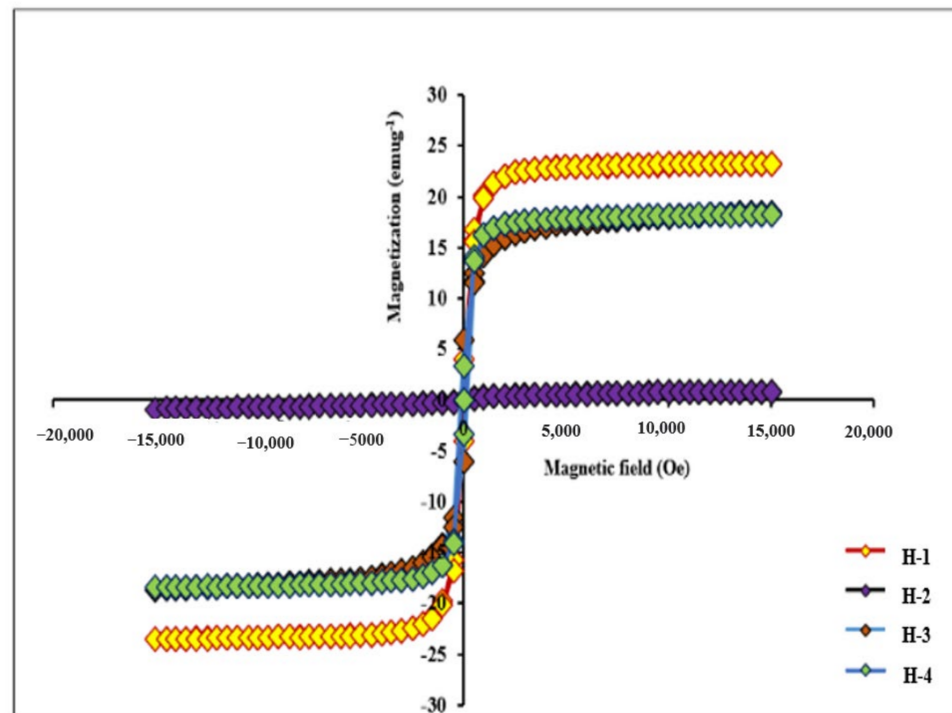


Figure 3. Magnetic Hysteresis loop of H-1 NPs; H-2 NPs; H-3 NPs; H-4 NPs.

Table 2. Saturation Magnetization, Coercivity, Retentivity of H-1, H-2, H-3 and H-4 NPs.

NPs/(NC)	Saturation Magnetization (M_s) (emu g^{-1})	Retentivity (M_r) (emu g^{-1})	Coercivity (H_c) (Oe)
H-1 NPs	23.34	4.05	103.4
H-2 NPs	0.86	0.12	213.4
H-3 NC	19.53	5.96	170.6
H-4 NC	18.48	3.44	99.1

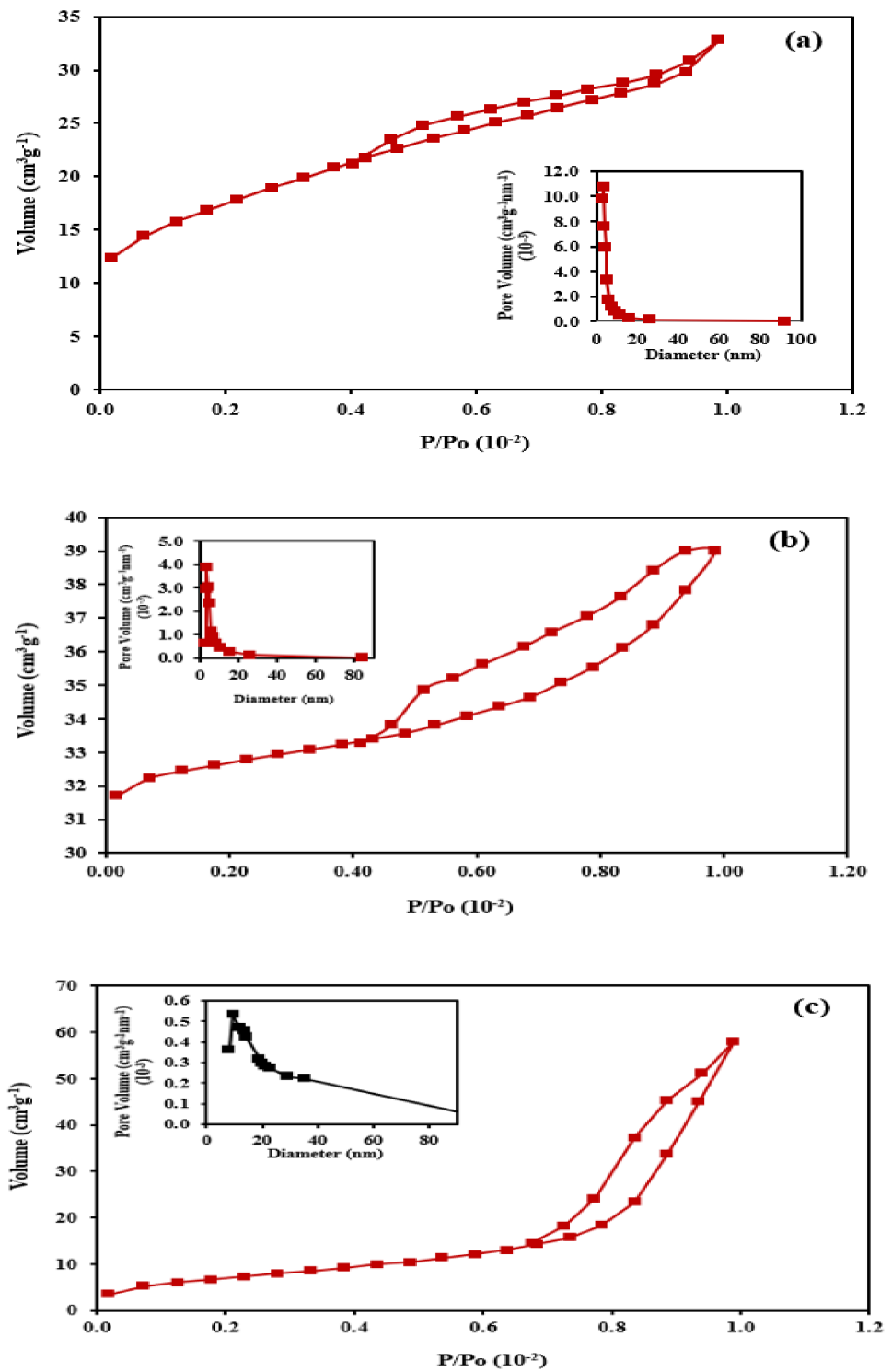


Figure 4. Cont.

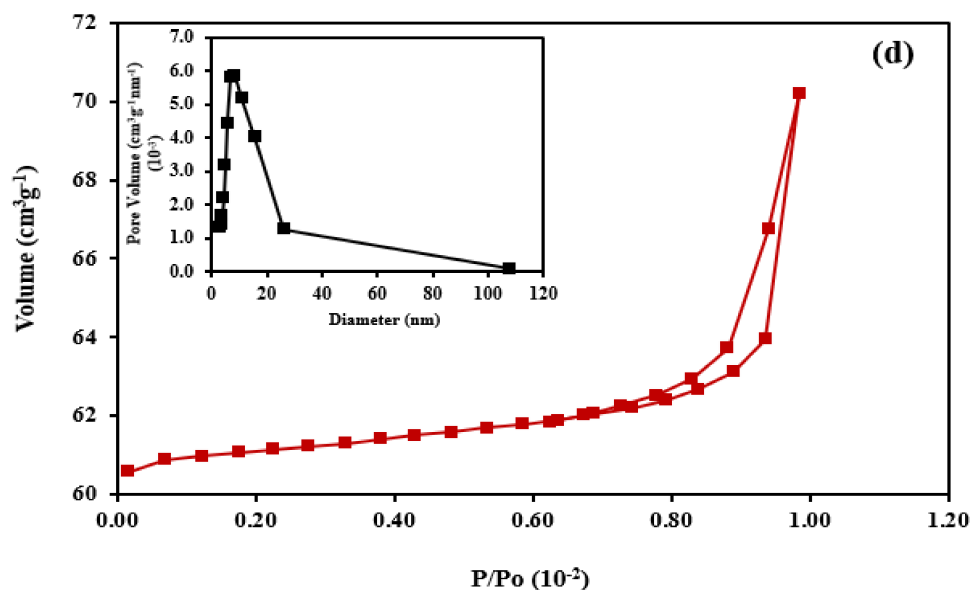


Figure 4. Adsorption—desorption N₂ graphs and corresponding pore size distribution (inset) of (a) H-1 NPs (b) H-2 NPs (c) H-3 NPs (d) H-4 NPs.

Table 3. BET: The NPs' specific surface area.

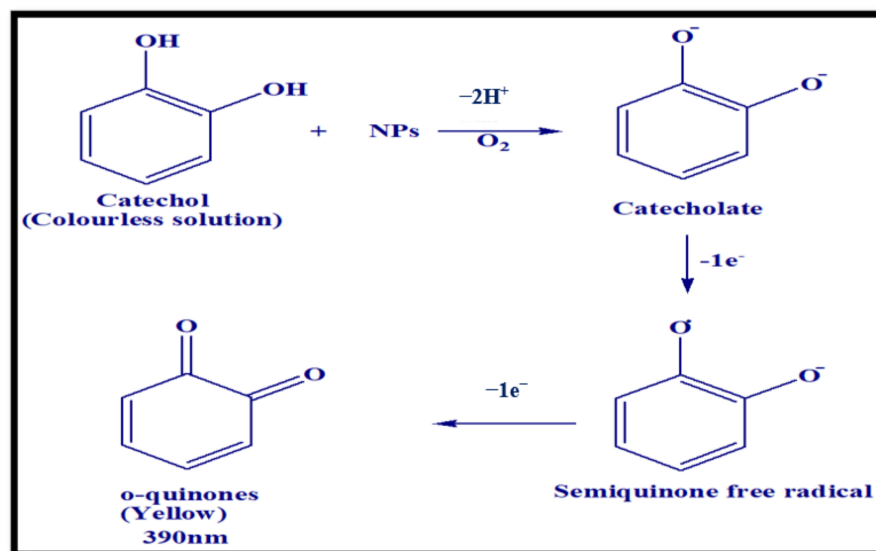
NPs/NC	BET Surface Area (m ² g ⁻¹)	Pore Volume (ccg ⁻¹)	Pore Diameter (nm)
H-1 NPs	32.81	0.03	3.11
H-2 NPs	38.98	0.12	3.51
H-3 NC	53.03	0.17	9.88
H-4 NC	70.17	0.18	11.61

3.2. PPO-Mimic Activity

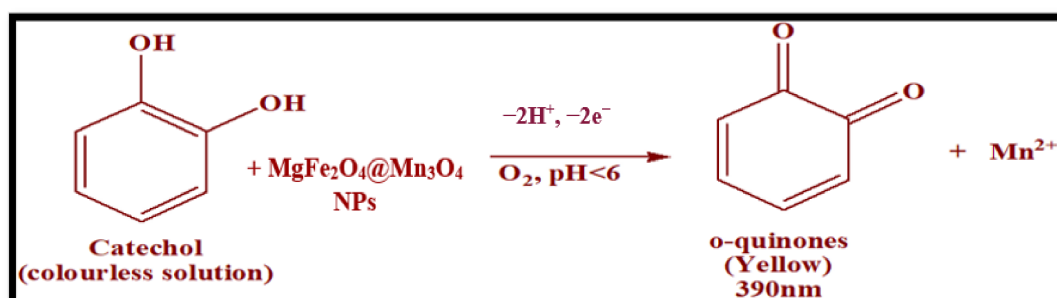
Due to the presence of MgFe₂O₄ the surface area of nanocomposite increased which resulted in greater interaction with substrate causing enhanced enzyme mimic activity. Since PPO-like activity is also dependent on electron transfer, the substrates transfer their electron to NPs by electron transfer to form catecholate/resorcinolate, which subsequently generates o-quinones and 1,3-Benzoquinone via electron transfer in the presence of dissolved O₂ (Schemes 3 and S1). Among NPs and nanocomposite, H-4 NC displayed the highest activity followed by H-3 and H-2 (Figure S4). Lowest activity was shown by H-1 NPs. These results indicate that in the nanocomposite Mn₃O₄ is the catalytic centre. These results revealed that at lower MgFe₂O₄ concentration as in H-4 NC the activity was increased due to lesser agglomeration of NPs. PPO activity also depends upon electron transfer process and surface area but electron transfer process was dominated. Without electron transfer process, catechol cannot be reduced to catecholate further into semiquinone free radicals and o-quinone [40–43]. Mn³⁺ is expected to gain an electron in Mn₃O₄ (Mn²⁺O.Mn³⁺₂O₃) NPs through direct coordination of catecholate with metal into unoccupied sigma orbital (3d⁴ to 3d⁵), with no change in spin state during electron transfer. Mn³⁺ is reduced to Mn²⁺ by accepting an electron from catechol. The presence of MgFe₂O₄ increased the surface area of the nanocomposite as depicted in Scheme 4.

Iron (Fe) has an electronic configuration of [Ar] 3d⁶4s², but in MgFe₂O₄ NPs, iron is present as Fe³⁺, which already has a stable electronic configuration of 3d⁵, thus it cannot take an electron from catechol and hence cannot participate in the electron transfer process, resulting in no reaction [44]. The activity of H-3 NC was lowered as compared to H-4 NC because higher content of MgFe₂O₄ hampered the electron transfer process. Catechol and resorcinol solutions were characterized by an λ_{max} peak at 285 nm and 274 nm. The

oxidation of catechol and resorcinol in the presence nanocomposite was determined spectrophotometrically by the formation of o-quinones which showed absorbance at 390 nm. Increase in absorbance directly correlated with the PPO-mimic activity. Higher the absorbance, more is the PPO-like activity. As H-4 NC showed the best activity among all the synthesized samples. Further experiments were performed using this nanocomposite.



Scheme 3. Mechanism of PPO mimic activity using catechol as a substrate.



Scheme 4. Process of electron transfer between catechol and Mn₃O₄ NPs.

Different parameters impacting enzyme mimic activity were studied, with the findings displayed in Figure 5. Figure 5a shows the effect of changing the pH of the solution from 1.0 to 9.0 on nanozyme activity. At pH 1.0, the nanocomposite activity peaked. After pH 3.0, the activity dropped dramatically. The stability of semiquinone free radicals at high pH was the cause of the reduction in activity. However, in order to avoid the acidic conditions pH 3.0 was optimized for further experiments. Temperature had an effect on activity, as shown in Figure 5b, with the maximum activity being recorded at 25 °C and the reaction rate was decreased when temperature was increased, indicating that 25 °C was the ideal temperature. Since less catecholate/resorcinolate was oxidized to semiquinone free radicals as the temperature increased, the formation of surface complexes between catechol/resorcinol and nanocomposite reduced. Similarly, the concentration of substrate and the dose of NC were investigated (Figure 5c,d). The optimal substrate dosage was observed to be 2 mg. There were less semiquinone radicals at extremely low concentrations of catechol and resorcinol, resulting in decreased activity, but catechol/resorcinol at higher concentrations has inadequate capacity to completely oxidize to semiquinone radicals, resulting in build-up of semiquinone radicals. The most effective dose was found to be 5 mg. When the dose was increased up to 5 mg, the activity of nanocomposite increased, but when the concentration of nanocomposite exceeded the ideal limit, it caused diminished

activity. 10 min was found to be the ideal contact time (Figure 5e). Since as the time of contact increased, a greater number of NPs interacted with the substrate, the activity of the NC increased, and thus the absorbance increased. Curve flattened after reaching its peak at 10 min, and no more increase is observed after this point [45].

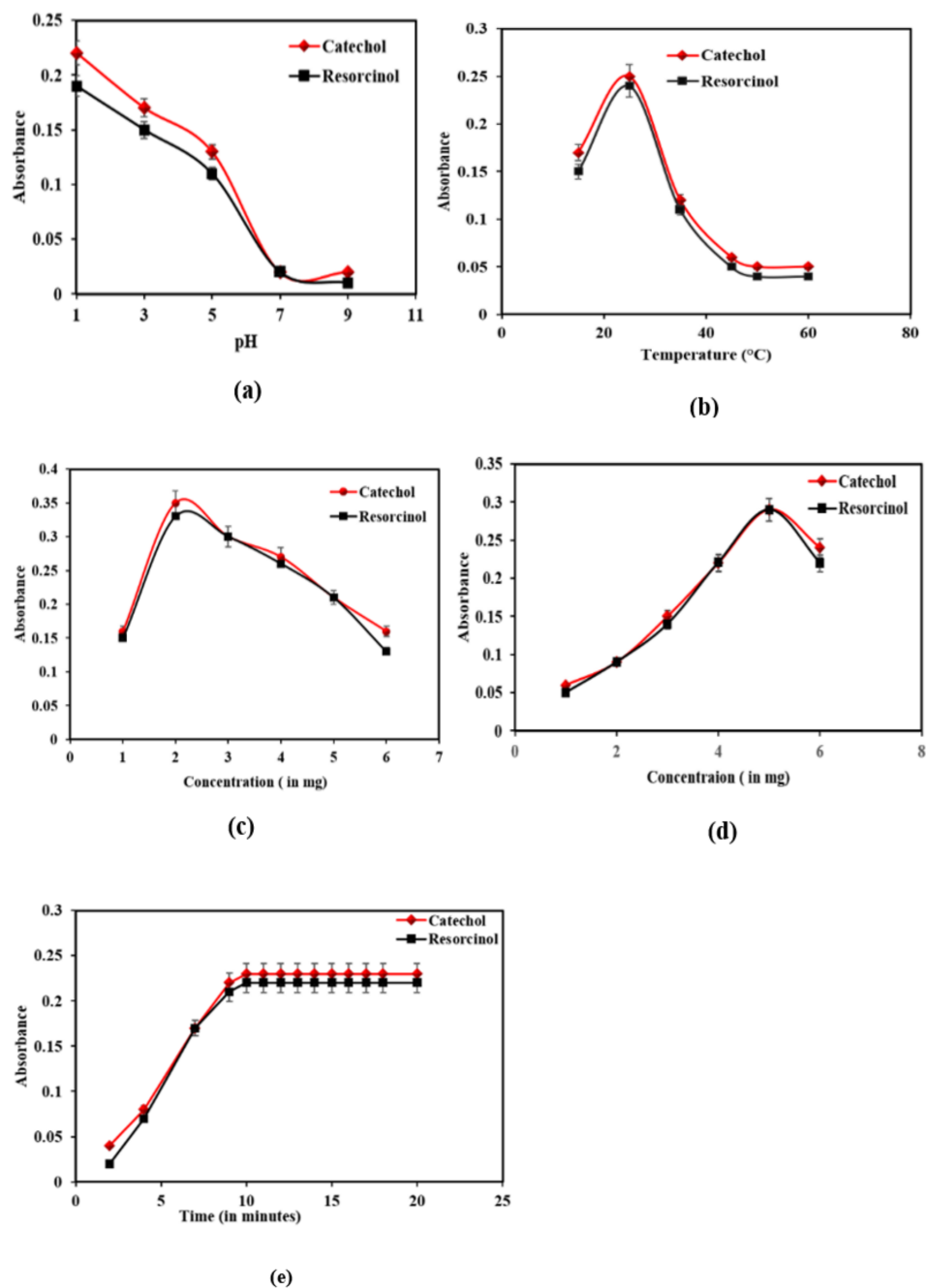


Figure 5. Factors affecting PPO-mimic activity (a) Effect of pH (b) Effect of temperature (c) Effect of substrate concentration (d) Effect of H-4 NPs concentration (e) Effect of contact time (pH = 3.0 at 25 °C and 0.5 mL H₂O₂).

3.3. Kinetic Studies of PPO-Like Activity and Recyclability Test

The variation in the absorbance of the reaction at 390 nm was monitored for 5 min at 1 min intervals for varied dosages of catechol and resorcinol. The change in catechol and resorcinol absorbance at varied concentrations of nanocomposite is shown in Figure 6a,b. The rate constants were determined for various concentrations using $\log [A_0/(A_0 - A_t)]$,

where A_0 and A_t indicate the absorbance levels at infinite time and time “ t ”, respectively. The reaction of nanocomposite followed first-order kinetics at low substrate concentrations and zero order kinetics at higher substrate concentrations, as shown in Figure S5a,b. The kinetic parameters K_m and V_{max} were calculated from the Lineweaver-Burk plot shown in Figure S6a,b, (Table S3). K_m is an indicator of the enzyme affinity to the substrate. As nanocomposite has lower value of K_m (app) = 0.7 mM as compared to Mn_3O_4 (K_m (app) = 1.14 mM) therefore, nanocomposite has higher enzyme affinity to bind to the substrate. Presence of Mn_3O_4 facilitated electron transfer process and presence of $MgFe_2O_4$ increased the surface area of the NC. As a result, a decreased K_m value indicated that synthesized NC as effective PPO mimics.

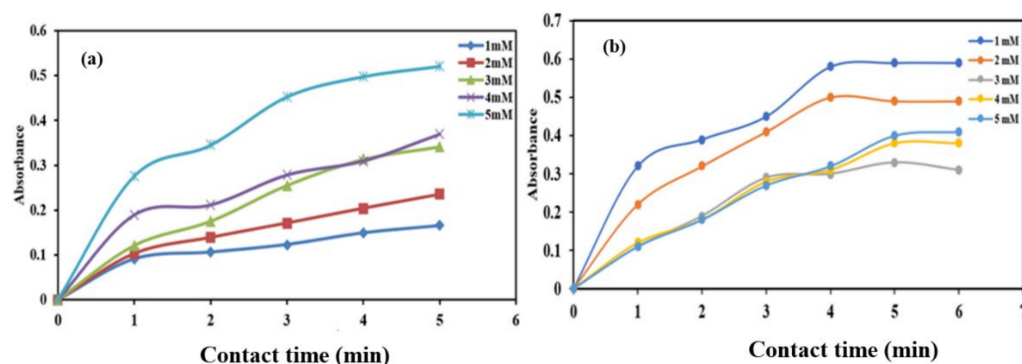


Figure 6. (a) Plot of change absorbance vs. time for various doses of nanocomposite using (a) catechol (b) resorcinol (pH = 3.0 at 25 °C, and 0.5 mL H_2O_2).

Figure 7 shows the reusability result, which shows that after four cycles, 79 percent of the PPO-mimicking activity was preserved. The loss of sample amount throughout each cycle resulted in a drop in mimic activity. CTAB@ $MgFe_2O_4$ nanocomposite as peroxidase mimic were found to have a comparable drop in activity by Singh et al., 2021 [24]. After six months of storage at room temperature, the catalytic activity of the synthesized nanocomposite remained unaltered, showing the nanocomposite persistence as PPO-mimic.

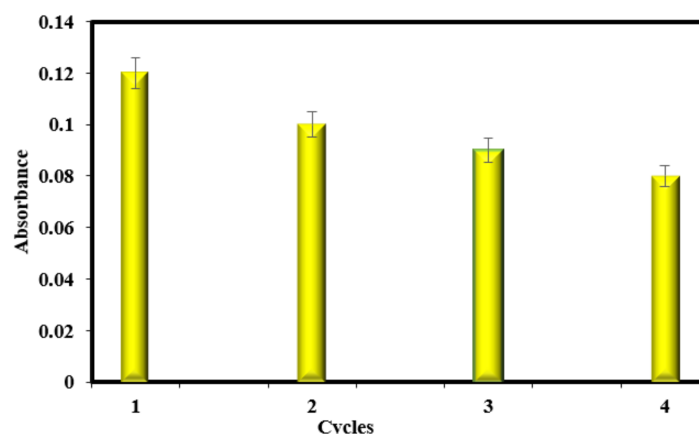


Figure 7. Recyclability test with repeated cycles (pH = 3.0 at 25 °C, and 0.5 mL H_2O_2).

3.4. Mechanism of PPO Mimic Activity

Naturally occurring PPO contains copper and the enzyme is involved in catalyzing the oxidation of polyphenolic compounds. The ability of nanocomposite to act as a PPO-mimic by catalyzing the oxidation of the usual PPO substrate catechol and resorcinol was proven in this study. In comparison to natural PPO, nanocomposite showed superior stability. Catechol and resorcinol release their hydroxyl hydrogen to the PPO-mimic, forming catechol and resorcinolate, which consequently result in formation of semiquinone free

radicals via electron transfer. In the case of nanocomposite, electron gain by Mn^{3+} (catalytic centre) was most likely accomplished via direct coordination of catecholate with metal, with no change in spin state. Mn^{3+} is reduced into Mn^{2+} by receiving an electron from catecholate/resorcinolate. The role of $MgFe_2O_4$ is to increase the surface area of the nanocomposite which enhanced activity of nanocomposite as compared to pristine Mn_3O_4 NPs. In addition to the contact and interaction between enzyme mimic and substrates, electron transport occurs in the catalytic core, which is a significant element in controlling the reaction rate [27]. This study is the first look at the enzyme mimicking activity of $MgFe_2O_4@Mn_3O_4$ nanocomposite.

3.5. The Statistical Analysis Findings

The Box-Behnken statistical model was employed using the detailed input data listed in Table 4. (Four independent variables and 30 runs). This table shows the actual and expected catechol and resorcinol concentrations, as well as the experimental design matrix for the Box-Behnken statistical model. As a result, a quadratic model was developed to estimate enzyme activity of nanocomposite using catechol and resorcinol extracted from aqueous solution. The quadratic models for catechol and resorcinol are shown in Tables S4 and S5, respectively. This model can be written as shown in Equations (2) and (3) with 4 coded factors for catechol and resorcinol, respectively, as:

$$\text{Absorbance (Using catechol)} = 2.05 - 0.1167A - 0.0167B + 0.000C - 0.1167D + 0.0500AD + 0.2750BD + 0.2375C^2 - 0.2625D^2 \quad (2)$$

$$\text{Absorbance (Using resorcinol)} = 2.17 + 0.1250 A - 0.0583 B - 0.0667 C - 0.0333D + 0.4250 AB + 0.4250CD \quad (3)$$

Table 4. Results of analysis of variance for the enzyme activity of nanocomposite using catechol and resorcinol.

Runs	pH	Temperature	Catalyst Dose	Contact Time	Absorbance (Catechol)	Absorbance (Resorcinol)
1	5	10	6	11	1.9	1.8
2	5	60	3.5	20	1.8	1.9
3	5	35	3.5	11	1.9	2
4	5	35	3.5	11	2	2.2
5	1	10	3.5	11	2.2	2.5
6	1	35	6	11	2.5	1
7	5	10	1	11	2.5	1.8
8	5	60	3.5	2	1.5	1.9
9	9	35	3.5	20	1.8	2
10	5	60	1	11	2.2	2.2
11	5	35	1	2	2.3	2.5
12	5	10	3.5	20	1.6	2.5
13	9	35	3.5	2	1.2	1.5
14	1	35	3.5	20	1.1	1.8
15	5	35	3.5	11	2	2.2
16	5	35	3.5	11	2	2.3
17	5	35	6	2	2	1.6
18	1	60	3.5	11	2.5	1.2
19	5	35	1	20	2.2	1.1
20	9	35	1	11	2	2
21	5	35	3.5	11	1.9	2
22	9	10	3.5	11	1.9	2
23	5	60	6	11	2.3	2.5
24	5	10	3.5	2	2.4	2.2
25	1	35	1	11	2	2
26	5	35	6	20	2	1.9
27	1	35	3.5	2	2.5	1.9
28	5	35	3.5	11	2.5	2.3
29	9	60	3.5	11	2	2.4
30	9	35	6	11	2.5	2

The normal probability versus plot of residuals from the least-squares fitting for the response catechol and resorcinol, is graphically depicted in Figures S7a and S8a. The points on the plot are also quite near to a straight line since the residuals follow a normal distribution pattern. In Figures S7b and S8b, a random scatter plot of the actual values and expected findings of catechol and resorcinol is shown. Both the expected and actual results are distributed randomly around the 45° straight line, suggesting that the error values between the actual and anticipated values have a zero mean. All of these findings point to the proposed model's strong correlation and appropriateness in predicting enzyme mimic activity using catechol and resorcinol.

3.6. Standardization of the Experimental Parameters

The optimization procedure's purpose is to find a set of experimental variable levels where enzyme activity (as measured by catechol and resorcinol) is at its peak. This is accomplished using the Box-Behnken design process, which is an excellent technique for determining the optimal operating conditions among a range of experimental variables evaluated. The results showed that the suggested model properly predicted the best enzyme activity utilizing catechol and resorcinol under optimal conditions, which included pH = 1.0; temperature = 25 °C; catalyst dose = 5 mg; and contact time = 10 min. Enzyme mimic was studied activity using catechol as substrate at pH ranging from 1–9, with variation in contact time = 2–20 min (Figure 8a) and using resorcinol as substrate at temperature ranging from 10–60 °C, with variation in pH (Figure 8b). The factor of desirability was 1 which represents a desirable, or ideal response (Figure 9). These graphs show that as the contact time grows up to a certain point, strong enzyme mimic activity occurs at acidic pH values [46]. Another crucial aspect to investigate is the dose of catalyst nanoparticles, as it may have a substantial impact on the performance of enzyme mimic activity. Furthermore, from an economical perspective, determining the optimal catalyst quantity is one of the most important attributes. The enzyme mimic activity increased with increasing NP dosage and contact time up to a specific limit, as shown in Figure 8b. An increase in the amount of PPO-mimic in the solution causes this behaviour, which increases the surface area or reaction sites.

3.7. Colorimetric Detection of Catechol and Resorcinol

Catechol and resorcinol were determined using a sensitive and straightforward approach. The variations in absorbance spectra in the presence of catechol at various concentrations shown in Figures 10a and 11a (0.1 mM to 0.8 mM) at 25 °C at 390 nm using H-4, i.e., MgFe₂O₄@Mn₃O₄ (1:2) nanocomposite solution of pH 3.0 with the addition of 0.5 mL H₂O₂ into respective solutions. With increasing catechol content, the absorbance increased in a consistent manner. The linear connection between catechol concentration and system absorption intensity is shown in Figure S9a, with both proportionate to each other in the range of 0.1–0.8 mM ($R^2 = 0.986$) and a detection limit of 0.29. This technique, as anticipated, might also be utilized to identify resorcinol. The absorbance spectra variations in the presence of resorcinol (0.01 to 0.08 mM) using H-4 NC solution having temperature 25 °C with pH 3.0 at 390 nm are represented in Figures 10b and 11b. It's clear that when the concentration of resorcinol rises, so does the absorbance of the solution. The relationship between the strength of absorption and the concentration of resorcinol in the solution is shown in Figure S9b, with both being proportionate in the range of 0.01–0.08 mM ($R^2 = 0.926$) and a detection limit of 0.03. Table 5 summarizes the efficacy of different PPO-mimic for catechol and resorcinol detection. The other polyphenol oxidase biosensors include electrochemical sensors using PEDOT-Gr/Ta electrode for the measurement of hydroquinone, catechol, resorcinol and nitrite [47]. Likewise, fluorescence-based sensing using titanium dioxide (P-TiO₂) nanoparticles (NPs) and fluorescein, has been used for sensing of catechol [48]. The novelty of present work is colorimetric sensing of polyphenols. The role of MgFe₂O₄@Mn₃O₄ nanocomposite is that it catalyzes the oxidation of catechol and resorcinol to semiquinones and gives faint brownish colour depending upon

the concentration of polyphenol which is the basis for colorimetric sensing application. The colorimetric biosensor showed a stable increase in colour intensity with increasing catechol and resorcinol concentration at pH =3.0. However, it is more sensitive for resorcinol showing faint pink to brownish colour and the biosensor gives light brown colour for catechol. The colorimetric biosensor using $\text{MgFe}_2\text{O}_4@\text{Mn}_3\text{O}_4$ nanocomposite has advantage of being simple, portable and easy to use.

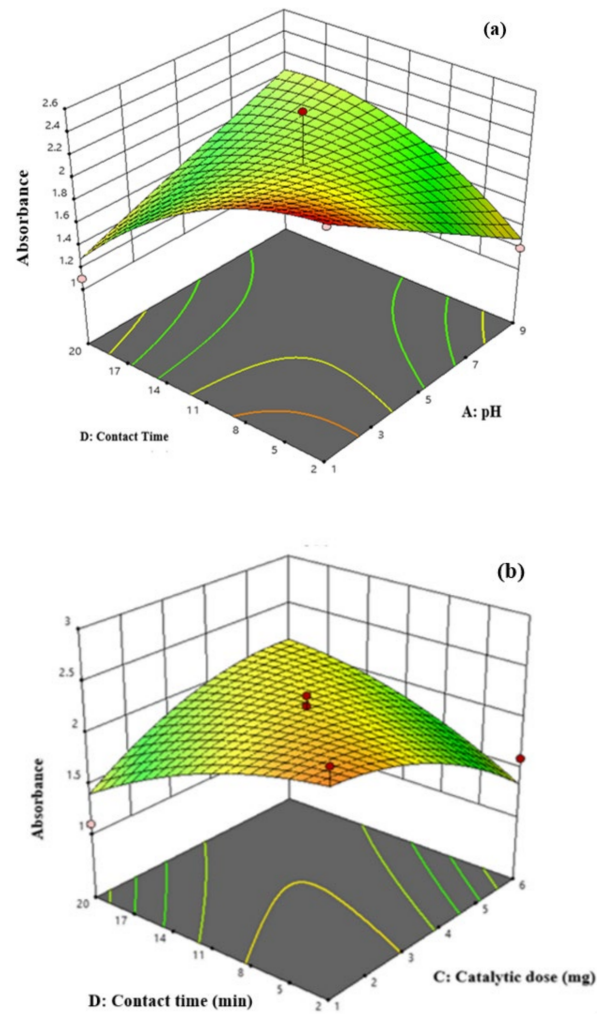


Figure 8. (a) Enzyme activity of nanocomposite (using catechol) as a function of contact time and pH. (b) Enzyme activity of nanocomposite (using resorcinol) as a function of contact time and catalytic dose.

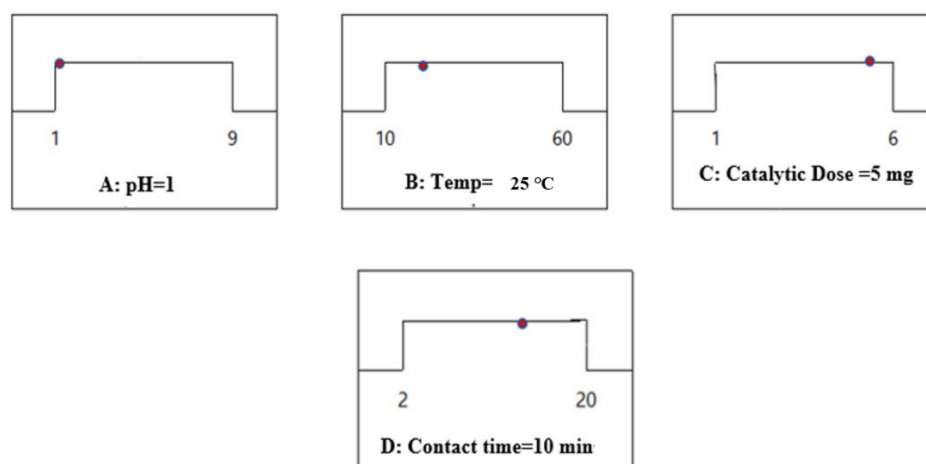


Figure 9. The Box-Behnken statistical method to create optimal conditions of pH, temperature, catalytic dose and contact time.

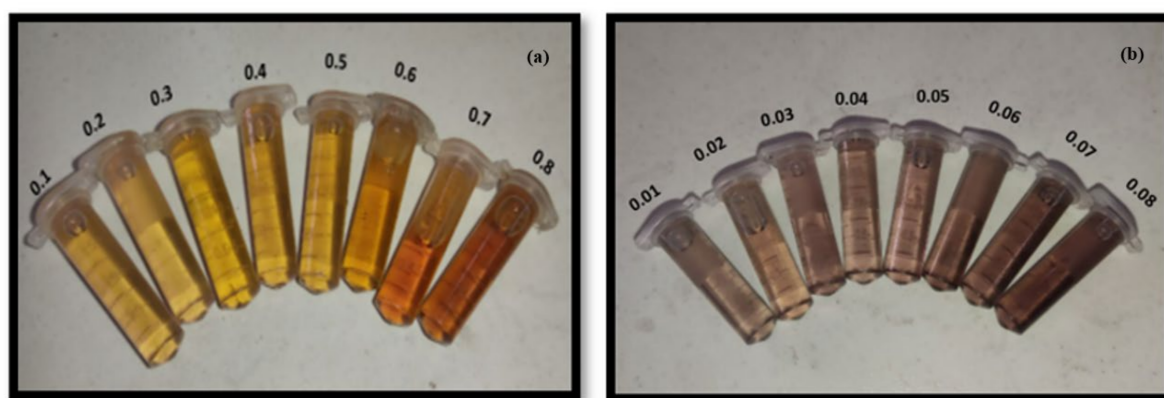


Figure 10. Different concentrations in mM of (a) Catechol (b) Resorcinol.

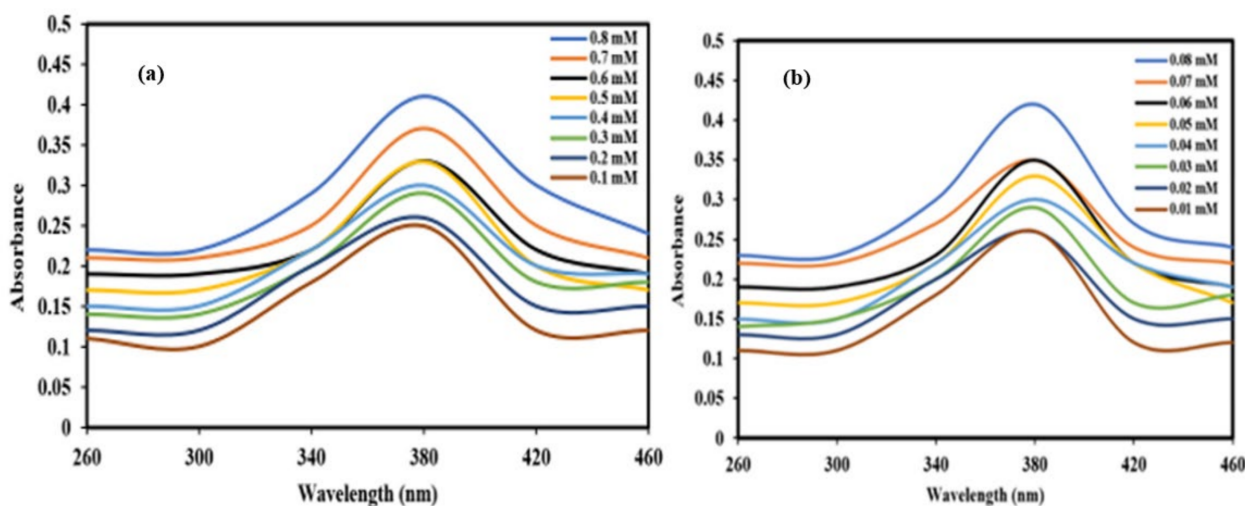


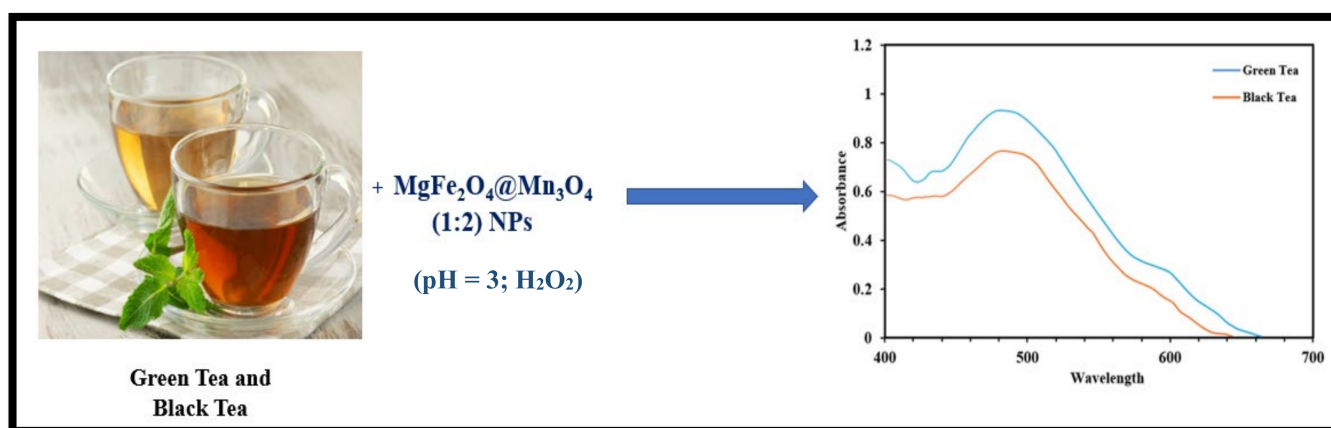
Figure 11. (a) The UV-vis absorbance spectra changes in the presence of catechol (0.8 mM, 0.7 mM, 0.6 mM, 0.5 mM, 0.4 mM, 0.3 mM, 0.2 mM, and 0.1 mM). ($\text{MgFe}_2\text{O}_4@ \text{Mn}_3\text{O}_4$ (1:2) nanocomposite solution of pH 3.0 at 25 °C) (b): The UV-vis absorbance spectra changes in the presence of resorcinol (0.01 mM, 0.02 mM, 0.03 mM, 0.04 mM, 0.05 mM, 0.06 mM, 0.07 mM, and 0.08 mM). ($\text{MgFe}_2\text{O}_4@ \text{Mn}_3\text{O}_4$ (1:2) nanocomposite solution of pH 3.0 at 25 °C).

Table 5. Range and limit of detection (LOD) for catechol and resorcinol by various PPO-mimics.

Sample	Substrate	Method	Linear Range (μM)	Detection Limit (μM)	References
PEDOT-Gr	Resorcinol	Electrochemical	6–200 μM	0.16 μM	[47]
P-TiO ₂ NPs	Resorcinol	Fluorescent	0.5–100 μM	0.092 μM	[48]
SWCNT/GCE	Resorcinol	Voltammetry	5–80 μM	1.0 μM	[49]
GCE	Resorcinol	Electrochemical	1–300 μM	0.75 μM	[50]
H-4 NC	Catechol	Colorimetric	0.1–0.8 mM	0.2 mM	Present work
H-4 NC	Resorcinol	Colorimetric	0.01–0.08 mM	0.03 mM	Present work

3.8. Colorimetric Sensing of Polyphenols in Tea Samples

Two samples of green and black tea were used in the assay, and the results were compared to those obtained using traditional methods. The colorimetric sensing of polyphenols in tea samples in the presence of $\text{MgFe}_2\text{O}_4@\text{Mn}_3\text{O}_4$ in the wavelength ranging from 400–700 nm was used to determine the total phenolic content of aqueous green and black tea extracts. The total phenolic content ($R^2 = 0.0995$) measured by the Folin-Ciocalteu assay, which comes out to be 62.2 mg/100 mL and 44.5 mg/100 mL, has a statistically significant linear association with the results from the study of two different tea types using nanocomposite as 63.3 mg/100 mL and 45.3 mg/100 mL for green tea and black tea, respectively (Figure 12). The role of $\text{MgFe}_2\text{O}_4@\text{Mn}_3\text{O}_4$ (1:2) nanocomposite is that it catalyzes the oxidation of polyphenols which are present in green and black tea extracts into quinones [28,51,52]. In order to ascertain the complex phenolic composition of tea such as catechin, esculetin, caffeic acid and rutin the advanced analytical approaches consisting of both LC-LTQ-Orbitrap Fourier transformed (FT)-MS and LC-time-of-flight-(TOF)-MS coupled to solid-phase extraction (SPE) NMR have been reported [53]. The elaborated chromatographic method enabled separation, qualitative and quantitative determination of five catechins (C, EC, EGC, EGCG and ECG) and gallic acid, the main phenolic acid, which esterifies polyphenols in tea [54]. However, the present study was focussed on facile estimation of total phenolic content of tea samples by colorimetric method using synthesized $\text{MgFe}_2\text{O}_4@\text{Mn}_3\text{O}_4$ nanocomposite as PPO-mimic.

**Figure 12.** UV-vis spectra of $\text{MgFe}_2\text{O}_4@\text{Mn}_3\text{O}_4$ nanocomposite with tea extracts of green and black tea at pH = 3.0.

4. Conclusions

The $\text{MgFe}_2\text{O}_4@\text{Mn}_3\text{O}_4$ nanocomposite-based platform could be used to detect catechol and resorcinol in the range of 0.1–0.8 mM and 0.01–0.08 mM, respectively, under optimized conditions, with detection limits of 0.20 mM for catechol and 0.03 Mm for resorcinol. The findings of the tea variety study show a statistically significant linear correlation

with total phenolic content ($R^2 = 0.0995$) as measured by the Folin-Ciocalteu test. These findings indicate that $\text{MgFe}_2\text{O}_4@\text{Mn}_3\text{O}_4$ nanocomposite with optimized ratio can be used for colorimetric sensing of polyphenols. Furthermore, $\text{MgFe}_2\text{O}_4@\text{Mn}_3\text{O}_4$ nanocomposite as PPO mimics shown several advantages over natural PPO enzyme, including ease of synthesis, storage, and stability. The nanocomposite can be employed as PPO mimics in a variety of applications, including biosensing and polyphenolics removal in industrial waste waters. The results afford platform for potential applications of the developed system in different fields such as clinical diagnosis and environmental monitoring of polyphenols.

Supplementary Materials: The following supporting information can be downloaded at: <https://www.mdpi.com/article/10.3390/bios12060428/s1>, Table S1: Details of characterization techniques; Table S2. Variables, level of design experiments, and Box-Behnken Design (for catechol and resorcinol); Figure S1: FT-IR spectra of H-1, H-2, H-3 and H-4 NPs; Figure S2: SEM EDS of (a) H-1 NPs (b) H-2 NPs (c) H-3 NC; Figure S3: TEM of (a) H-1 NPs (b) H-2 NPs; Figure S4: Comparison of activity of different samples; Scheme 1. Mechanism of PPO activity using resorcinol; Figure S5: Plot of initial rates versus substrate concentration of oxidation catalysed by H-4 nanocomposite (a) Catechol (b) Resorcinol; Figure S6: The lineweaver burk plot for H-4 NC (a) Catechol (b) Resorcinol; Table S3: Kinetic parameters for PPO-like activity mention in text discuss; Table S4: Analyses of variance for quadratic model of catechol; Table S5. Analysis of variance for quadratic model of resorcinol; Figure S7: (a) Correlation between the experiments with predicted values of enzyme activity (using catechol), (b) Normal probability plot of residuals obtained by ANOVA for the enzyme activity of H-4 nanocomposite (using catechol); Figure S8: Correlation between the experiments with predicted values of enzyme activity (using resorcinol), (b) Normal probability plot of residuals obtained by ANOVA for the enzyme activity of H-4 nanocomposite (using resorcinol); Figure S9: The linear calibration plots for (a) catechol detection b) resorcinol detection; Figure S10: Calibration plot of total phenolic content determined by the $\text{MgFe}_2\text{O}_4@\text{Mn}_3\text{O}_4$ nanocomposite based assay. References [55,56] are cited in the supplementary materials.

Author Contributions: H.K. formal analysis, experimental plan, preparation of the manuscript draft; M.K. conceptualization, writing-review, editing, analysis of results, validation; R.A. analysis of results, validation, review and editing; S.S. writing-review and editing, analysis of results, D.S. statistical analysis, review and editing. All authors have read and agreed to the published version of the manuscript.

Funding: This research received no external funding.

Institutional Review Board Statement: Not applicable.

Informed Consent Statement: Not applicable.

Data Availability Statement: Supporting data available.

Conflicts of Interest: The authors declare no conflict of interest.

References

1. Daniel, R.M.; Dines, M.; Petach, H.H. The denaturation and dehydration of stable enzyme at high temperatures. *Biochem. J.* **1996**, *317*, 1–11. [[CrossRef](#)]
2. Batista, C.A.S.; Larson, R.G.; Kotov, N.A. Nonadditivity of nanoparticle interactions. *Science* **2015**, *350*, 1242477. [[CrossRef](#)]
3. Long, M.; Jiang, J.; Li, Y.; Cao, R.; Zhang, L.; Cai, W. Effect of gold nanoparticles on the photocatalytic and photoelectrochemical performance of Au modified BiVO_4 : Effective inorganic photocatalysis for H_2O_2 production from H_2O and O_2 under visible light. *Nano-Micro Lett.* **2011**, *3*, 171–177. [[CrossRef](#)]
4. Natalio, F.; Andre, R.; Hartog, A.F.; Stoll, B.; Jochum, K.P.; Wever, R.; Tremel, W. Vanadium pentoxide nanoparticles mimic vanadium halo peroxidases and thwart biofilm formation. *Nat. Nanotechnol.* **2012**, *7*, 530–535. [[CrossRef](#)] [[PubMed](#)]
5. Shi, W.; Wang, Q.; Long, Y.; Cheng, Z.; Chen, S.; Zheng, H.; Huang, Y. Carbon nanodots as peroxidase mimetics and their applications to glucose detection. *Chem. Comm.* **2011**, *47*, 6695–6697. [[CrossRef](#)] [[PubMed](#)]
6. He, S.; Huang, Y.; Huang, J.; Liu, W.; Yao, T.; Jiang, S.; Tang, F.; Liu, J.; Hu, F.; Pan, Z.; et al. Ultrathin CoOOH oxides nanosheets realizing efficient photocatalytic hydrogen evolution. *J. Phys. Chem. C* **2015**, *119*, 26362–26366. [[CrossRef](#)]
7. Dumore, N.S.; Mukhopadhyay, M. Sensitivity enhanced SeNPs -FTO electrochemical sensor for hydrogen peroxide detection. *J. Electroanal. Chem.* **2020**, *878*, 114544. [[CrossRef](#)]

8. Wu, C.W.; Unnikrishnan, B.; Tseng, Y.T.; Wei, S.C.; Chang, H.T.; Huang, C.C. Mesoporous manganese oxide/manganese ferrite nanopopcorns with dual enzyme mimic activities: A cascade reaction for selective detection of ketoses. *J. Colloid Interface Sci.* **2019**, *541*, 75–85. [[CrossRef](#)]
9. Wang, X.; Zhao, M.; Song, Y.; Liu, Q.; Zhang, Y.; Zhuang, Y.; Chen, S. Synthesis of ZnFe₂O₄/ZnO heterostructures decorated three-dimensional graphene foam as peroxidase mimetics for colorimetric assay of hydroquinone. *Sens. Actuator. B Chem.* **2019**, *283*, 130–137. [[CrossRef](#)]
10. Valko, M.; Leibfritz, D.; Moncol, J.; Cronin, M.T.; Mazur, M.; Telser, J. Free radicals and antioxidants in normal physiological functions and human disease. *Int. J. Biochem. Cell. Biol.* **2007**, *39*, 44–84. [[CrossRef](#)]
11. Lertvachirapaiboon, C.; Kiyokawa, I.; Baba, A.; Shinbo, K.; Kato, K. Colorimetric determination of hydrogen peroxide based on localized surface plasmon resonance of silver nanoprisms using a microchannel chip. *Anal. Lett.* **2019**, *52*, 1939–1950. [[CrossRef](#)]
12. Du, H.; Zhang, X.; Liu, Z.; Qu, F. A supersensitive biosensor based on MoS₂ nanosheet arrays for the real-time detection of H₂O₂ secreted from living cells. *Chem. Commun.* **2019**, *55*, 9653–9656. [[CrossRef](#)]
13. Yu, J.; Cao, M.; Wang, H.; Li, Y. Novel manganese (II)-based metal-organic gels: Synthesis, characterization and application to chemiluminescent sensing of hydrogen peroxide and glucose. *Microchim. Acta* **2019**, *186*, 696. [[CrossRef](#)]
14. Yang, Y.; Mao, Z.; Huang, W.; Liu, L.; Li, J.; Li, J.; Wu, Q. Redox enzyme-mimicking activities of CeO₂ nanostructures: Intrinsic influence of exposed facets. *Sci. Rep.* **2016**, *6*, 35344. [[CrossRef](#)]
15. Ashour, A.H.; El-Batal, A.I.; Maksoud, M.A.; El-Sayyad, G.S.; Labib, S.; Abdeltwab, E.; El-Okri, M.M. Antimicrobial activity of metal-substituted cobalt ferrite nanoparticles synthesized by sol-gel technique. *Particuology* **2018**, *40*, 141–151. [[CrossRef](#)]
16. Verma, V.; Kaur, M.; Sharma, S. Superoxide dismutase mimic activity of spinel ferrite MFe₂O₄ (M=Mn, Co and Cu) nanoparticles. *Bull. Mater. Sci.* **2019**, *42*, 120.
17. Hosseini, M.; Sabet, F.S.; Khabbaz, H.; Aghazadeh, M.; Mizani, F.; Ganjali, M.R. Enhancement of the peroxidase-like activity of cerium-doped ferrite nanoparticles for colorimetric detection of H₂O₂ and glucose. *Anal. Methods* **2017**, *9*, 3519–3524. [[CrossRef](#)]
18. Moccellini, S.K.; Fernandes, S.C.; De Camargo, T.P.; Neves, A.; Vieira, I.C. Self-assembled monolayer of nickel(II) complex and thiol on gold electrode for the determination of catechin. *Talanta* **2009**, *78*, 1063–1068. [[CrossRef](#)]
19. Ulbrich, K.D.F.; Winiarski, P.J.; Jost, C.L.; De Campos, C.E.M. Green and facile solvent-free synthesis of NiTe₂ nanocrystalline material applied to voltammetric determination of antioxidant morin. *Mater. Today Commun.* **2020**, *25*, 101251. [[CrossRef](#)]
20. De Carvalho, M.L.; Santhiago, M.; Peralta, R.A.; Neves, A.; Mücke, G.A.; Vieira, I.C. Determination of chlorogenic acid in coffee using a biomimetic sensor based on a new tetranuclear copper (II) complex. *Talanta* **2008**, *74*, 394–399. [[CrossRef](#)]
21. Navadeepthy, D.; Rebekah, A.; Viswanathan, C.; Ponpandian, N. N-doped Graphene/ZnFe₂O₄: A novel nanocomposite for intrinsic peroxidase based sensing of H₂O₂. *Mater. Res. Bull.* **2017**, *95*, 1–8.
22. Su, L.; Feng, J.; Zhou, X.; Ren, C.; Li, H.; Chen, X. Colorimetric detection of urine glucose based ZnFe₂O₄ magnetic nanoparticles. *Anal. Chem.* **2012**, *84*, 5753–5758. [[CrossRef](#)]
23. Garg, D.; Kaur, M.; Sharma, S.; Verma, V. Effect of CTAB coating on structural, magnetic and peroxidase mimic activity of ferric oxide nanoparticles. *Bull. Mater. Sci.* **2018**, *41*, 134. [[CrossRef](#)]
24. Singh, E.; Kaur, M.; Sharma, S. Stuning of CTAB@MgFe₂O₄ nanocomposite as peroxidase mimic for H₂O₂ and glucose sensing. *Mat. Chem. Phys.* **2021**, *271*, 124851. [[CrossRef](#)]
25. Gatselou, V.; Christodouleas, D.C.; Kouloumpis, A.; Gournis, D.; Giokas, D.L. Determination of Phenolic Compounds Using Spectral and Color Transitions of Rhodium Nanoparticles. *Anal. Chim. Acta* **2016**, *932*, 80–87. [[CrossRef](#)]
26. Singh, M.; Kaur, M.; Sangha, M.K.; Ubhi, M.K. Comparative evaluation of manganese oxide and its graphene oxide nanocomposite as polyphenol oxidase mimics. *Mater. Today Commun.* **2021**, *27*, 102237. [[CrossRef](#)]
27. Verma, V.; Kaur, M.; Sharma, S. Insight into peroxidase and polyphenol oxidase mimic activity of spinel ferrite nanoparticles and their GO composites. *Mater. Chem. Phys.* **2022**, *279*, 125727. [[CrossRef](#)]
28. Liebert, M.; Licht, U.; Bohm, V.; Bitsch, R. Antioxidative properties and total phenolic content of green and black tea under different brewing conditions. *Eur. Food Res. Technol.* **1999**, *208*, 217–220.
29. Kaur, M.; Singh, M.; Mukhopadhyay, S.S.; Singh, D.; Gupta, M. Structural, magnetic and adsorptive properties of clay ferrite nanocomposite and its use for effective removal of Cr (VI) from water. *J. Alloys Compd.* **2015**, *653*, 202–211. [[CrossRef](#)]
30. Zauberman, G.; Ronen, R.; Akerman, M.; Weksler, A.; Rot, I.; Fuchs, Y. Postharvest retention of the red colour of litchi fruit pericarp. *Sci. Hort.* **1991**, *47*, 89–97. [[CrossRef](#)]
31. Bazrafshan, E.; Al-Musawi, T.; Silva, F.M.; Panahi, A.H.; Havangi, M.; Mostafapur, F.K. Photocatalytic degradation of catechol using ZnO nanoparticles as catalyst: Optimizing the experimental parameters using the Box-Behnken statistical methodology and kinetic studies. *Microchem. J.* **2019**, *147*, 643–653. [[CrossRef](#)]
32. Kaur, N.; Kaur, M. Comparative studies on impact of synthesis methods on structural and magnetic properties of magnesium ferrite nanoparticles. *Process. Appl. Ceram.* **2014**, *8*, 137–143. [[CrossRef](#)]
33. Spiers, H.; Parkin, I.P.; Pankhurst, Q.A.; Affleck, L.; Green, M.; Caruana, D.J.; Kvick, A. Self propagating high temperature synthesis of magnesium zinc ferrites (Mg_xZn_{1-x}Fe₂O₃): Thermal imaging and time resolved X-ray diffraction experiments. *J. Mater. Chem.* **2004**, *14*, 1104–1111. [[CrossRef](#)]
34. Trivedi, M.K.; Branton, A.; Trivedi, D.; Nayak, G.; Bairwa, K.; Jana, S. Spectroscopic Characterization of Disodium Hydrogen Orthophosphate and Sodium Nitrate after Biofield Treatment. *J. Chromatogr. Sep. Tech.* **2015**, *6*, 1000282. [[CrossRef](#)]

35. Yang, L.X.; Liang, Y.; Chen, H.; Meng, Y.F.; Jiang, W. Controlled synthesis of Mn_3O_4 and $MnCO_3$ in a solvothermal system. *Mat. Res. Bull.* **2009**, *44*, 1753–1759. [[CrossRef](#)]
36. Wang, L.; Li, Y.; Han, Z.; Chen, L.; Qian, B.; Jiang, X.; Pinto, J.; Yang, G. Composite structure and properties of Mn_3O_4 /graphene oxide and Mn_3O_4 /graphene. *J. Mater. Chem. A* **2013**, *1*, 8385–8397. [[CrossRef](#)]
37. Olmos, A.V.; Redon, R.; Gattorno, G.R.; Zamora, M.E.M.; Leal, F.M.; Osorio, A.L.F.; Saniger, J.M. One step synthesis of Mn_3O_4 nanoparticles: Structural and magnetic study. *J. Colloid Interface Sci.* **2005**, *291*, 175–180. [[CrossRef](#)]
38. Pradeep, A.; Priyadharsini, P.; Chandrasekaran, G. Sol–gel route of synthesis of nanoparticles of $MgFe_2O_4$ and XRD, FTIR and VSM study. *J. Magn. Magn. Mater.* **2008**, *320*, 2774–2779. [[CrossRef](#)]
39. Zhang, Y.; Zhou, Z.; Wen, F.; Tan, J.; Peng, T.; Luo, B.; Yin, S. A flower-like MoS_2 -decorated $MgFe_2O_4$ nanocomposite: Mimicking peroxidase and colorimetric detection of H_2O_2 and glucose. *Sens. Actuator B Chem.* **2018**, *275*, 155–162. [[CrossRef](#)]
40. Cullity, B.D. Some problems in X-ray stress measurements. *Adv. X-ray Anal.* **1976**, *20*, 259–271. [[CrossRef](#)]
41. Singh, R.P.; Venkataraju, C. Effect of calcinations on the structural and magnetic properties of magnesium ferrite nanoparticles prepared by sol gel method. *China J. Phys.* **2018**, *56*, 2218–2225. [[CrossRef](#)]
42. Torelli, S.; Belle, C.; Hamman, S.; Pierre, J.L.; Saint-Aman, E. Substrate binding in catechol oxidase activity: Biomimetic approach. *Inorg. Chem.* **2002**, *41*, 3983–3989. [[CrossRef](#)]
43. Basak, T.; Ghosh, K.; Chattopadhyay, S. Synthesis, characterization and catechol oxidase mimicking activity of two iron(III) Schiff base complexes. *Polyhedron* **2018**, *146*, 81–92. [[CrossRef](#)]
44. Thankachan, S.; Jacob, B.P.; Xavier, S.; Mohammed, E.M. Effect of neodymium substitution on structural and magnetic properties of magnesium ferrite nanoparticles. *Phys. Scr.* **2013**, *87*, 025701. [[CrossRef](#)]
45. Ono, Y.; Matsumura, T.; Fukuzumi, S. Electron spin resonance studies on the mechanism of the formation of p-benzosemiquinone anion over manganese dioxide. *J. Chem. Soc.* **1977**, *2*, 1421–1424.
46. Kumari, P.V.K.; Yarraguntla, S.R.; Sharmila, M.; Gulbindala, E. Application of Box-Behnken Design for Formulation Parameters of Eslicarbazepine Tablets. *Indian J. Pharm. Sci.* **2021**, *83*, 575–583. [[CrossRef](#)]
47. Tian, F.; Li, H.; Li, M.; Li, C.; Lei, Y.; Yang, B. Synthesis of one dimensional poly(3,4-ethylenedioxythiophene)-graphene composites for the simultaneous detection of hydroquinone, catechol, resorcinol, and nitrite. *Synth. Met.* **2017**, *226*, 148–156. [[CrossRef](#)]
48. Wu, H.P.; Cheng, T.L.; Tseng, W.L. Phosphate-modified TiO_2 nanoparticles for selective detection of dopamine, levodopa, adrenaline, and catechol based on fluorescence quenching. *Langmuir* **2007**, *23*, 7880–7885. [[CrossRef](#)]
49. Ding, Y.; Liu, W.; Wu, Q.S.; Wang, X.G. Direct simultaneous determination of dihydroxybenzene isomers at C-nanotube modified electrodes by derivative voltammetry. *J. Electroanal. Chem.* **2005**, *575*, 275–280. [[CrossRef](#)]
50. Yin, H.; Zhang, Q.; Zhou, Y.; Ma, Q.; Liu, T.; Zhu, L.; Ai, S. Electrochemical behavior of catechol, resorcinol and hydroquinone at graphene–chitosan composite film modified glassy carbon electrode and their simultaneous determination in water samples. *Electrochim. Acta* **2011**, *56*, 2748–2753. [[CrossRef](#)]
51. Szydłowska-Czerniak, A.; Laszewska, A.; Tulodziecka, A. A novel iron oxide nanoparticle-based method for the determination of the antioxidant capacity of rapeseed oils at various stages of the refining process. *Anal. Methods* **2015**, *7*, 4650–4660. [[CrossRef](#)]
52. Scroccarello, A.; Pelle, F.D.; Neri, L.; Pittia, P.; Compagnone, D. Silver and gold nanoparticles based colorimetric assays for the determination of sugars and polyphenols in apples. *Food Res. Int.* **2019**, *119*, 359–368. [[CrossRef](#)] [[PubMed](#)]
53. Van der Hoft, J.J.J.; Akermi, M.; Unlu, F.Y.; Mihaleva, V.; Roldan, V.G.; Bino, R.J.; de Vos, R.C.H.; Vervoort, J. Structural Annotation and Elucidation of conjugated phenolic compounds in black, green and white tea extracts. *Agric. Food Chem.* **2012**, *60*, 8841–8850. [[CrossRef](#)] [[PubMed](#)]
54. Koch, W.; Kukula-Koch, W.; Komsta, L.; Marzec, Z.; Szwerc, W.; Glowniak, K. Green tea quality evaluation based on its catechins and metal composition in combination with chemometric analysis. *Molecules* **2018**, *23*, 1689. [[CrossRef](#)]
55. Lee, J.W.; Yoon, S.; Lo, Y.M.; Wu, H.; Lee, S.Y.; Moon, B. Intrinsic polyphenol oxidase-like activity of gold platinum nanoparticles. *RSC Adv.* **2015**, *5*, 63757–63764. [[CrossRef](#)]
56. Liu, Y.; Wu, H.; Chong, Y.; Wamer, W.G.; Xia, Q.; Cai, L.; Nie, Z.; Fu, P.; Yin, J.J. Platinum nanoparticles: Efficient and stable catechol oxidase mimetics. *ACS Appl. Mater. Interfaces* **2015**, *7*, 19709–19717. [[CrossRef](#)]